Stable Visual Servoing Through Hybrid Switched-System Control

Nicholas R. Gans, *Member, IEEE*, and Seth A. Hutchinson, *Fellow, IEEE*

***Abstract*—Visual servoing methods are commonly classified as image-based or position-based, depending on whether image features or the camera position define the signal error in the feedback loop of the control law. Choosing one method over the other gives asymptotic stability of the chosen error but surrenders control over the other. This can lead to system failure if feature points are lost or the robot moves to the end of its reachable space.**

We present a hybrid switched-system visual servo method that utilizes both image-based and position-based control laws. We prove the stability of a specific, state-based switching scheme and present simulated and experimental results.

***Index Terms*—Switched-system control, vision based control, visual servoing.**

I. Introduction

VISUAL servo control allows for the closed-loop control of a robot end effector through the use of image data. It provides a high degree of accuracy using even simple camera systems and offers robustness in the face of signal error and uncertainty of system parameters.

Classically, there have been two approaches to visual servo control: Image-Based Visual Servoing (IBVS) and Position-Based Visual Servoing (PBVS). In IBVS, an error signal is measured in the image, and is mapped directly to actuator commands. In PBVS systems, features are detected in an image and used to estimate the current camera position. A position error is then computed in the Cartesian task space, and this error is used by the control system. There has been a great deal of research on each of these [1]–[8].

Chaumette outlined a number of problems that cannot be solved using the traditional local linearized approaches to visual servo control [9]. Many of these problems are fundamental to the control law. For example, by zeroing the error in the image space, IBVS provides no control over the specific position or velocity of the camera and may perform unnecessary motions that can lead to system failure. Likewise, PBVS surrenders control of the image features, which may allow them to leave the image, in which case pose reconstruction may be impossible. Tasks that fail can be well posed initially, so detection of impending failure is often impossible.

A number of partitioned approaches have been introduced to address these problems [10]–[13]. These approaches partition the system's degrees of freedom into disjoint sets, each of which is controlled by a different control scheme. Partitioning the visual servo system along specific degrees of freedom of motion gives access to new, potentially better, trajectories for the system.

Other methods to address one or more of these problems have been introduced as well. Taylor and Ostrowski [14] introduced a unique, PBVS-like controller based on the fundamental matrix relating camera views. This system was shown to be asymptotically stable even with large calibration errors. Cowan, *et al.* [15], presented visual servoing methods based on the use of navigation functions, similar to artificial potential functions. This system can avoid loss of feature points and incorporate boundaries on the robot pose, in terms of distance from the camera to the features. Mezouar and Chaumette [16] developed an IBVS path planner to keep the pose error minimal while keeping the features in the field of view. Kyrki *et al.* [17] developed a PBVS controller that maintained target visibility while following a minimum distance path in Cartesian space by allowing freedom in the orientation to keep the object in the field of view. Garcia-Aracil *et al.*, [18] allow feature points to leave and enter the field of view while maintaining a smooth control law.

We have proposed a new hybrid switched-system approach [19], [20], in which system control is partitioned along the time axis rather than along specific dimensions of the state space. A hybrid switched system comprises a set of continuous subsystems along with a discrete switching controller that switches between them [21], [22]. Using hybrid switched systems, it may be possible to increase the region of stability, increase the rate of convergence, and to switch between unstable systems in a pattern that makes the total system stable. Taking a simple view of performance, IBVS performs well when PBVS performs badly, and vice versa. Thus, rather than mitigating bad performance along particular degrees of freedom (as with the partitioned methods), we attempt to improve performance over time.

We present a switching strategy that achieves stability in both the pose space and image space simultaneously. More importantly, it is possible to specify neighborhoods for the image error and pose error that the state can never leave. This insures that no

Manuscript received April 6, 2006; revised November 17, 2006. This paper was recommended for publication by Associate Editor P. Rives and Editor F. Park upon evaluation of the reviewers' comments. This material is based in part upon work supported by the National Science Foundation under Awards CCR-0085917 and IIS-0083275.

N. R. Gans is with the Department of Mechanical and Aerospace Engineering, University of Florida, Gainesville, FL 32579 USA (e-mail: ngans@ufl.edu).

S. A. Hutchinson is with the Department of Electrical and Computer Engineering, University of Illinois at Urbana-Champaign, Urbana, IL 61801 USA (e-mail: seth@uiuc.edu).

Color versions of one or more of the figures in this paper are available online at http://ieeexplore.ieee.org.

Digital Object Identifier 10.1109/TRO.2007.895067

feature ever leaves the image, and the robot never moves beyond a specified distance to the goal pose. This is a strong result, and to our knowledge, no other VS controller can guarantee never to fail due to these reasons.

Recently, a few other switching approaches have been introduced as well. Chesi and Vicino [23] introduced a switched-system PBVS controller that keeps features in the field of view by switching to a different PBVS controller when the features approach the edge of the image. Deng, *et al.* [24], presented a system that switches between to PBVS to avoid singularities and local minima in the IBVS control law. In the same paper, they developed an off-line path planner that incorporates image, Cartesian and joint space constraints and avoids singularities and local minima in the IBVS control law.

We present a simple set of switching rules to facilitate the analysis of the system. However, our switched system is inclusive to additional switching rules. For instance, alternate or additional switching surfaces could be introduced to avoid collisions in a known workspace. A switched system could also incorporate methods developed in [24] to escape local minima and singularities in the image Jacobian, or switch to controllers like those in [25] and [26] to avoid joint limits and joint space singularities.

The remainder of the paper is organized as follows. Section II provides a brief review of hybrid switched systems and IBVS and PBVS methods. Section III describes our new hybrid switched-system controller, which incorporates both an IBVS controller and a PBVS controller. Section IV contains the proofs of stability for our state-based switching method. Results of experiments are given in Section V.

II. Background

In this section, we provide background information on hybrid systems and visual servoing. These topics are well covered in literature. Our purpose here is to introduce notation and quickly summarize relevant results.

A. Hybrid Switched-System Control

The theory of hybrid, switched control systems, i.e., systems that comprise a number of continuous subsystems and a discrete system that switches between them, has received notable attention in the control theory community [21], [22], [27], [28]. In general, a hybrid switched system can be represented by the differential equation

$$\dot{x}(t) = f_{\sigma(t)}(x,t) : \sigma \in \{1 \dots n\} \tag{1}$$

where f_σ is a collection of n distinct functions. The solution to (1) is a pair $\{x(t), \sigma(t)\}$ giving the value of the state and switching variable, respectively, over time. The functions $x(t)$ and $\sigma(t)$ are continuous from the right to insure both are locally Lipschitz.

For our purposes, it is convenient to explicitly note that the switching behavior can directly affect the choice of the control input u

$$\dot{x}(t) = f_{\sigma(t)}\left(x, t, u_{\sigma(t)}\right) : \sigma \in \{1 \dots n\}. \tag{2}$$

A useful interpretation is to consider σ to be a discrete signal, switching among discrete values in $\{1 \dots n\} \subseteq \mathbb{Z}_+$. The value σ at time t determines which function $f_\sigma(x, u_\sigma)$ governs system behavior at time t. The signal σ is often classified as state-dependent or dependent, depending on whether switching is caused by the state of x or the time t, although these classifications are not firm and can overlap.

The stability of a switched system is not insured by the stability of the individual controllers. Indeed, a collection of stable systems can become unstable when inappropriately switched [27], [29].

Furthermore, stability of a switched system can be extremely difficult to prove. For a specific switching rule, stability can be established through a finite family of Lyapunov functions [29], [30]. This will be discussed further in Section IV-B. It is generally more difficult to prove stability under arbitrary switching. This generally requires finding a common Lyapunov function for all subsystems [27], [31]. This will be discussed in further detail in Section IV-A.

B. Position-Based Visual Servoing

The task in PBVS is to regulate the error between the current camera pose and the goal pose. Given a current camera pose $\mathbf{X}(t)$ and goal pose $\mathbf{X}^*$ (throughout the paper, the superscript * denotes values at the goal configuration), the transformation relating them is described by a translation $\mathbf{d} \in \mathbb{R}^3$ and rotation of the camera frame $\mathbf{R} \in SO(3)$.

Locally, $SO(3)$ can be parameterized by the three-tuple $\mathbf{u}\theta$, in which θ is an angle of rotation about the axis defined by the unit vector $\mathbf{u}$. Given a collection of feature points in the image, there are numerous methods to extract $\mathbf{X}(t)$ and thus $\mathbf{d}$ and $\mathbf{u}\theta$ from $\mathbf{X}(t)$ [32]–[34].

For a PBVS system, we define the error $\mathbf{e}_\mathrm{p}$ in terms of the rigid body motion that relates $\mathbf{X}$ to $\mathbf{X}^*$

$$\mathbf{e}_\mathrm{p} = \begin{bmatrix} \mathbf{d} \\ \mathbf{u}\theta \end{bmatrix}. \tag{3}$$

If the camera is moving with velocity $\xi = (\mathbf{v}^T, \omega^T)^T$ (in twist coordinates) the relationship between the error derivative and the camera velocity is given by

$$\dot{\mathbf{e}}_\mathrm{p} = \begin{bmatrix} \mathbf{R} & 0 \\ 0 & \mathbf{L}_\omega \mathbf{R} \end{bmatrix} \xi = \mathbf{L}_p \xi \tag{4}$$

in which [10]

$$\mathbf{L}_\omega(\mathbf{u}, \theta) = I - \frac{\theta}{2}\mathbf{u}_\times + \left(1 - \frac{\operatorname{sinc}\theta}{\operatorname{sinc}^2 \frac{\theta}{2}}\right)\mathbf{u}_\times^2 \tag{5}$$

and $\mathbf{u}_\times$ is the skew symmetric matrix associated with $\mathbf{u}$. Note that by definition, $\operatorname{sinc}(0) = 1$.

Since $\mathbf{L}_\omega$ is non singular when $\theta \neq k\pi$, $k \in \mathbb{Z} \setminus \{0\}$ [10], we can achieve the error dynamics $\dot{\mathbf{e}}_\mathrm{p} = -\lambda_\mathrm{p}\mathbf{e}_\mathrm{p}$, using a simple feedback control law

$$-\lambda_\mathrm{p}\mathbf{e}_\mathrm{p} = \dot{\mathbf{e}}_\mathrm{p} = \mathbf{L}_\mathrm{p}\xi \Longrightarrow \xi = -\lambda_\mathrm{p}\mathbf{L}_\mathrm{p}^{-1}\mathbf{e}_\mathrm{p} \tag{6}$$

in which λ_p is a positive gain scalar.

We use a quadratic candidate Lyapunov function

$$V_{\rm p}(\mathbf{e}_{\rm p}) = \frac{1}{2}\mathbf{e}_{\rm p}^T\mathbf{H}\mathbf{e}_{\rm p}, \quad \mathbf{H} = \begin{bmatrix} \eta\mathbf{I} & \mathbf{0} \\ \mathbf{0} & (1-\eta)\mathbf{I} \end{bmatrix} \tag{7}$$

$$V_{\rm p}(\mathbf{e}_{\rm p}) = \frac{1}{2}\left\|\mathbf{e}_{\rm p}(t)\right\|_{\rm H}^2 \tag{8}$$

where $\eta \in (0,1)$, $\mathbf{I}$ is a 3×3 identity matrix and $\mathbf{0}$ is a 3×3 matrix in which each element is 0. Different η allow us to scale effects of the translation with respect to rotation. We will typically use a large η to focus on the effects of position error without sacrificing the positive definiteness of V_p. For the case where $\eta = 0.5$, $\|\mathbf{e}_{\rm p}(t)\|_{\rm H}^2$ is a trivial scaling of the 2-norm.

When $\mathbf{L}_{\rm p}$ is full rank and $\eta \in (0.5, 1)$, it follows from (7) and (6) that

$$\begin{aligned} 0 \le V_{\rm p} &= \frac{1}{2}\mathbf{e}^T\mathbf{H}\mathbf{e} \\ V_{\rm p} &\le \frac{1}{2}\|\mathbf{e}\|\|\mathbf{H}\|\|\mathbf{e}\| \\ V_{\rm p} &\le \frac{\eta}{2}\|\mathbf{e}\|^2 \end{aligned} \tag{9}$$

and

$$\begin{aligned} \dot{V}_{\rm p} &= \mathbf{e}^T\mathbf{H}\dot{\mathbf{e}}_{\rm p} \\ &= \mathbf{e}^T\mathbf{H}(-\lambda_{\rm p}\mathbf{e}) \\ &\le -\lambda_{\rm p}(1-\eta)\|\mathbf{e}\|^2. \end{aligned} \tag{10}$$

A similar set of equations exists for the case that $\eta \in (0, 0.5)$. Thus, this controller is asymptotically stable for all translations $\mathbf{d} \in \mathbb{R}^3$ and rotation of the camera frame $\mathbf{R}(u,\theta)$ such that $\theta \in (-\pi, \pi)$. See [35] for a more detailed proof of stability and robustness.

Although the position error tends monotonically to zero, we cannot control the position of all the image points. If there is any rotation present, the feature points in the image will move along curves in the image plane as the camera undergoes rotation and translation. In a physical system with a limited imaging surface, it is possible for the feature points to leave the image. In this case, the system will fail to complete the task.

C. Image-Based Visual Servoing

With image-based visual servo control, the control law is a function of an error that is measured in the image. If $\mathbf{s}(t)$ denotes the vector of image features that are extracted from computer vision data, the error is defined in the image feature space, $\mathbf{e}_{\rm i}(t) = \mathbf{s}(t) - \mathbf{s}^*$. The relationship between camera velocity and the measured feature values is given by

$$\dot{\mathbf{s}} = \mathbf{L}_{\rm i}\xi \tag{11}$$

in which $\mathbf{L}_{\rm i}$ is the image Jacobian (also called the interaction matrix) [1]–[3], [7].

We can use a simple feedback control law

$$-\lambda_{\rm i}\mathbf{e}_{\rm i} = \dot{\mathbf{e}}_{\rm i} = \dot{\mathbf{s}} = \mathbf{L}_{\rm i}\xi \Longrightarrow \xi = -\lambda_{\rm i}\mathbf{L}_{\rm i}^+\mathbf{e}_{\rm i} \tag{12}$$

where $\mathbf{L}_{\rm i}^+ = (\mathbf{L}_{\rm i}^T\mathbf{L}_{\rm i})^{-1}\mathbf{L}_{\rm i}^T$ is the general inverse of $\mathbf{L}_{\rm i}$ and $\lambda_{\rm i}$ is a positive gain scalar.

Using the candidate Lyapunov function

$$V_{\rm i}(\mathbf{e}_{\rm i}) = \frac{1}{2}\left\|\mathbf{e}_{\rm i}(t)\right\|^2 \tag{13}$$

we obtain

$$\dot{V}_{\rm i} = -\lambda_{\rm i}\mathbf{e}_{\rm i}^T\mathbf{L}_{\rm i}\mathbf{L}_{\rm i}^+\mathbf{e}_{\rm i} \tag{14}$$

and we have asymptotic stability when the matrix $\mathbf{L}_{\rm i}\mathbf{L}_{\rm i}^+$ is positive definite.

Unfortunately, this condition is rarely achieved. When $\dim(\mathbf{s}) > 6$ the image Jacobian is overdetermined; it will have a nonempty null space, and local minima will exist [9]. However, when $\mathbf{L}_{\rm i}$ is full rank at the goal $\mathbf{s}^*$, then there is a neighborhood of $\mathbf{s}^*$ in which $\mathbf{L}_{\rm i}\mathbf{L}_{\rm i}^+$ is positive *semidefinite*, and thus IBVS is globally stable in the sense of Lyapunov, but not globally asymptotically stable. It can be shown that IBVS is locally asymptotically stable for some sufficiently small neighborhood of the origin, though to our knowledge the region of convergence has never been firmly established. See [3], [35], [36] for more detailed discussions of stability and robustness.

In addition to the problems of singularities and local minima, Chaumette has described problems that arise due to large physical camera motions that are sometimes required to follow IBVS-generated trajectories [9]. Thus, there are a number of serious performance problems that confront an IBVS system.

III. A Hybrid Switched-System Visual Servo Controller

We combine IBVS and PBVS controllers in a switched-system controller. To derive analytic results, we first establish a common state space within which both systems can be described. To this end we show that $\mathbf{e}_{\rm p}$ and $\mathbf{e}_{\rm i}$ are local coordinate charts of the pose error in $SE(3)$.

If a camera is posed with respect to a motionless set of feature points, the feature vector $\mathbf{s}$ can be defined as a mapping $\mathbf{s} = \pi(\mathbf{X})$, $\pi : SE(3) \mapsto \mathbb{R}^n$ from the camera pose to the image points using the well-known perspective projection function. Likewise, the pose error in $SE(3)$ can be mapped to the image error, $SE(3) \mapsto \mathbb{R}^n$, and through the local mapping of $SE(3) \mapsto \mathbb{R}^6$ described in Section II-B, there is a function from $\mathbf{e}_{\rm p}$ to $\mathbf{e}_{\rm i}$. We can therefor define $\mathbf{e}_{\rm i} = \pi'(\mathbf{e}_{\rm p})$, $\pi' : \mathbb{R}^6 \mapsto \mathbb{R}^n$.

It is easy to see that $\pi'(\mathbf{0}) = \mathbf{0}$. The matrix $\mathbf{L}_{\rm i}\mathbf{L}_{\rm p}^{-1}$ maps $\dot{\mathbf{e}}_{\rm p} \rightarrow \dot{\mathbf{e}}_{\rm i}$ (i.e. it maps the tangent space of $\mathbf{e}_{\rm p}$ to the tangent space of $\mathbf{e}_{\rm i}$). If $\operatorname{rank}(\mathbf{L}_{\rm i}) = 6$ at $\mathbf{e}_{\rm i} = \mathbf{0}$, then $\mathbf{L}_{\rm i}\mathbf{L}_{\rm p}^{-1}$ is full column rank and π' is locally injective in a neighborhood of $\mathbf{e}_{\rm p} = \mathbf{0}$. In this way, both $\mathbf{e}_{\rm p}$ and $\mathbf{e}_{\rm i}$ can be seen as local coordinates for the pose error in $SE(3)$. The inverse function of π (and π' by extension) can be computed by any of the many pose reconstruction routines for n feature points.

While $\mathbf{e}_{\rm p}$ and $\mathbf{e}_{\rm i}$ are both local coordinates of the pose error in $SE(3)$, it is usually more intuitive to think of them as separate, dependent measurements. In this spirit, we can map any error in $SE(3)$ to a point in $\mathcal{W} \subset \mathbb{R}^2$. This mapping is described by a function

$$W(\mathbf{e}_{\rm p}, \mathbf{e}_{\rm i}) = [w_1, w_2] = \left[\frac{1}{2}\|\mathbf{e}_{\rm i}\|^2, \frac{1}{2}\left\|\mathbf{e}_{\rm p}(t)\right\|_{\rm H}^2\right] \in \mathcal{W}. \tag{15}$$

In an abuse of terminology, we will refer to an analysis "in the space $\mathcal{W}$" to mean analyzing the map of $\mathbf{e}_{\rm p}$ and $\mathbf{e}_{\rm i}$ to $\mathcal{W}$.

We have designed a state-based switching visual servo controller that switches between controllers based on the values of the two Lyapunov functions given in (7) and (13). Given the locally injective map from $\mathbf{e}_\mathrm{p}$ to $\mathbf{e}_\mathrm{i}$, we note that (13) can be rewritten as

$$V_\mathrm{i}(\mathbf{e}_\mathrm{i}) = V_\mathrm{i}(\pi'(\mathbf{e}_\mathrm{p})) = V_\mathrm{i}'(\mathbf{e}_\mathrm{p}) \tag{16}$$

though we will rarely make the reliance of V_i on the pose error explicit.

To design our controller, we use level sets of these Lyapunov functions to define switching surfaces; when the system encounters these surfaces it will switch to the appropriate system. These level sets are defined by the constants $\gamma_\mathrm{p} > 0$ (which defines a maximum acceptable pose error) and $\gamma_\mathrm{i} > 0$ (which defines a maximum feature point error). The specific switching rule is given by:

- In IBVS mode, if $V_\mathrm{p}(\mathbf{e}_\mathrm{p}) \geq (1/2)\gamma_\mathrm{p}^2$, switch to PBVS mode.
- In PBVS mode, if $V_\mathrm{i}(\mathbf{e}_\mathrm{i}) \geq (1/2)\gamma_\mathrm{i}^2$, switch to IBVS mode.

The function W will map the level sets of V_p and V_i to straight lines in $\mathcal{W}$, and the interior of the intersection of the level sets will be mapped to a rectangle.

Under this control scheme, when using IBVS, the image error will decrease, but the pose error may increase. If the pose error becomes too large, the control switches to the PBVS controller. Analogously, when using PBVS the pose error will decrease, but the feature point error may increase. If the feature error becomes too large, the control switches to the IBVS controller.

Proofs of the stability of our system are given in Section IV. We are able to prove asymptotic stability within some sufficiently small neighborhood of zero pose and feature error. Within a known, defined neighborhood, we are able to prove stability, though not the stronger condition of asymptotic stability. In Section V, empirical evidence suggests that the switched system is attractive to the state $\mathbf{e}_\mathrm{i} = \mathbf{0}, \mathbf{e}_\mathrm{p} = \mathbf{0}$ over a large region.

IV. Analysis of Local Stability

We investigate the stability of our switched system. We are able to prove asymptotic stability within a neighborhood of the origin, however this neighborhood is not known. We are able to prove local stability in both the image error and pose error within neighborhoods of zero in both error spaces. More importantly, this neighborhood is defined explicitly by the user.

A. Local Asymptotic Stability Under Arbitrary Switching

We first show that in a sufficiently small neighborhood of the origin, a system arbitrarily switched between IBVS and PBVS will be asymptotically stable. It has been shown that if all systems in a family share a common Lyapunov function, the switched system is stable under arbitrary switching. We proceed to show that in a sufficiently small neighborhood, V_i is a common Lyapunov function for IBVS and PBVS

We assume that the feature points are stationary with respect to the world frame, that the image features are well posed so that the image Jacobian is full rank when the camera is at the goal pose, and that $V_\mathrm{i}(0) < (1/2)\gamma_\mathrm{i}^2$ and $V_\mathrm{p}(0) < (1/2)\gamma_\mathrm{p}^2$. These assumptions are typical in the visual servo literature (see, e.g., [35], [36]).

In the proof and in our simulations, we assume perfect camera calibration and that there is no signal noise. This grants perfect pose estimation and feature point depth estimation. In Section V, we present experiments on a real robot system to demonstrate stability of the system when these assumptions are relaxed.

Proposition: A hybrid switched-system visual servo system is asymptotically stable in the sense of Lyapunov under arbitrary switching within a sufficiently small neighborhood of the origin.

Proof: As discussed in Section III, there exists a function π' mapping $\mathbf{e}_\mathrm{p} \rightarrow \mathbf{e}_\mathrm{i}$, which is injective in a neighborhood of $\mathbf{e}_\mathrm{p} = \mathbf{0}$, and maps $\mathbf{e}_\mathrm{p} = \mathbf{0} \rightarrow \mathbf{e}_\mathrm{i} = \mathbf{0}$. In the region where π' is injective, the Jacobian $\mathbf{J} = (\partial\pi'/\partial\mathbf{e}_\mathrm{p})$ is full column rank. A Taylor expansion about $\mathbf{e}_\mathrm{p} = \mathbf{0}$ gives

$$\mathbf{e}_\mathrm{i} = \mathbf{J}(\mathbf{0})\mathbf{e}_\mathrm{p} + \mathcal{O}_2 \tag{17}$$

where $\mathcal{O}_2$ are terms second order and higher.

Combining (13) and (17) we get

$$V_\mathrm{i}(\mathbf{e}_\mathrm{i}) = \frac{1}{2}\mathbf{e}_\mathrm{i}^T\mathbf{e}_\mathrm{i} = \frac{1}{2}\mathbf{e}^T\mathbf{J}(\mathbf{0})^T\mathbf{J}(\mathbf{0})\mathbf{e}_\mathrm{p} + \mathcal{O}_2. \tag{18}$$

which is positive definite within a small neighborhood of the origin. Taking (6) and the derivative of (18), we see that under PBVS

$$\dot{V}_\mathrm{i} = \mathbf{e}^T\mathbf{J}(\mathbf{0})^T\mathbf{J}(\mathbf{0})\dot{\mathbf{e}}_\mathrm{p} \tag{19}$$

$$= -\lambda_\mathrm{p}\mathbf{e}^T\mathbf{J}(\mathbf{0})^T\mathbf{J}(\mathbf{0})\mathbf{e}_\mathrm{p} + \mathcal{O}_2, \tag{20}$$

which is negative definite in a neighborhood of the origin.

Section II-C showed that $V_\mathrm{i}(\mathbf{e}_\mathrm{i})$ is a valid Lyapunov function and proves global stability of $\mathbf{e}_\mathrm{i}$ under IBVS, and local asymptotic stability under IBVS within a sufficiently small neighborhood of the origin. Equation (20) shows that in a sufficiently small neighborhood of the origin V_i is also a valid Lyapunov function showing local asymptotic stability under PBVS. The intersection of these two neighborhoods is a neighborhood of the origin where V_i is a common Lyapunov function for IBVS and PBVS. [27]. □

B. Local Stability Through State Based Switching

In [29] Branicky gives a technique for establishing the stability of switched-control systems. For our system, we will use the two Lyapunov functions $V_\mathrm{p}(\mathbf{e}_\mathrm{p})$ and $V_\mathrm{i}(\mathbf{e}_\mathrm{i})$ defined in (7) and (13). We denote the set of switching times by $\mathcal{T} = \{t_0, t_1, t_2, \cdots\}$. Since we have exactly two controllers, the set of times at which the system switches to PBVS from IBVS is $\mathcal{T}_\mathrm{p} = \{t_1, t_3, \cdots\}$, and the set of times at which the system switches to IBVS from PBVS is $\mathcal{T}_\mathrm{i} = \{t_0, t_2, t_4, \cdots\}$.

For our specific system, the conditions for stability given in [29] are as follows:

1) $V_\mathrm{p}(0) = V_\mathrm{i}(0) = 0$.
2) $V_\mathrm{i}(\mathbf{e}_\mathrm{i}) > 0$ for $\|\mathbf{e}_\mathrm{i}\| \neq 0$ and $V_\mathrm{p}(\mathbf{e}_\mathrm{p}) > 0$ for $\|\mathbf{e}_\mathrm{p}\| \neq 0$.
3) $\dot{V}_\mathrm{i}(\mathbf{e}_\mathrm{i}(t)) \leq 0$ for $t_{2k} < t < t_{2k+1}$, for $k = 0, 1, 2\cdots$.
4) $V_\mathrm{i}(\mathbf{e}_\mathrm{i}(t_k)) \leq V_\mathrm{i}(\mathbf{e}_\mathrm{i}(t_l))$ for all $t_k, t_l \in \mathcal{T}_\mathrm{i}$ s.t. $t_l < t_k$.
5) $\dot{V}_\mathrm{p}(\mathbf{e}_\mathrm{p}(t)) \leq 0$ for $t_{2k-1} < t < t_{2k}$, for $k = 1, 2\cdots$.
6) $V_\mathrm{p}(\mathbf{e}_\mathrm{p}(t_k)) \leq V_\mathrm{p}(\mathbf{e}_\mathrm{p}(t_l))$ for all $t_k, t_l \in \mathcal{T}_\mathrm{p}$ s.t. $t_l < t_k$.

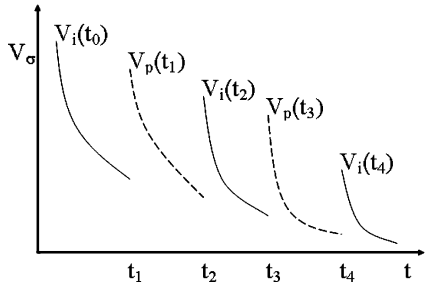

Fig. 1. Stable family of Lyapunov function.

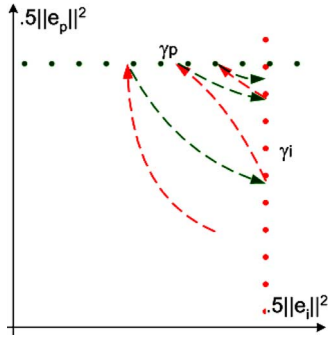

Fig. 2. A switching sequence that increases the error over time.

The first two conditions establish that each candidate Lyapunov function is positive definite in a neighborhood of the origin. The third and fourth conditions establish the Lyapunov-like property that $V_{\rm i}$ is nonincreasing when IBVS is active as well as at the switching instants for IBVS. The final two conditions establish the Lyapunov-like property that $V_{\rm p}$ is nonincreasing when PBVS is active as well as at the switching instants for PBVS. This is illustrated in Fig. 1, for a family of two Lyapunov functions. Function V_1 becomes active at switching times t_0, t_2 and t_4, while function V_2 becomes active at switching times t_1 and t_3. Furthermore $V_1(t_0) \geq V_1(t_2) \geq V_1(t_4)$ and $V_2(t_1) \geq V_2(t_3)$.

We now show that our hybrid switched system is stable in a known neighborhood. The proof assumes that the system begins with IBVS, but a proof for the system beginning with PBVS parallels this one.

Proposition: The hybrid switched-system visual servo system, with switching surfaces described by

- In IBVS mode, if $V_{\rm p}(\mathbf{e}_{\rm p}) \geq (1/2)\gamma_{\rm p}^2$, switch to PBVS mode
- In PBVS mode, if $V_{\rm i}(\mathbf{e}_{\rm i}) \geq (1/2)\gamma_{\rm i}^2$, switch to IBVS mode

is stable in the sense of Lyapunov within a well-defined neighborhood $\{\mathbf{X} \in (SE(3) | \mathbf{e}_{\rm p} < (1/2)\gamma_{\rm p}^2, \mathbf{e}_{\rm i} < (1/2)\gamma_{\rm i}^2\}$.

Proof:

- To establish that both $V_{\rm i}$ and $V_{\rm p}$ are positive definite in a neighborhood of the origin (conditions 1 and 2), it is sufficient to note that if $\mathrm{rank}(\mathbf{L}_{\rm i}) = 6$,

$$\mathbf{e_i} = 0 \Leftrightarrow \mathbf{e}_{\rm p} = 0$$

since any error in pose will cause an error in the observed image features, and conversely, an image error implies that there must be some pose error. Therefore, we have

$$V_{\rm i}(\mathbf{e}_{\rm i}) = V_{\rm p}(\mathbf{e}_{\rm p}) = 0 \Leftrightarrow \mathbf{e}_{\rm i} = \mathbf{e}_{\rm p} = 0.$$

Since both $V_{\rm i}$ and $V_{\rm p}$ are norms, they are positive definite. This satisfies conditions 1 and 2.

- Condition 3 follows from (14).
- Condition 4 requires two steps. First, $V_{\rm i}(\mathbf{e}_{\rm i}(t)) = (1/2)\gamma_{\rm i}^2$ for all $t \in \mathcal{T}_{\rm i} \setminus \{t_0\}$. Branicky showed that his method can be extended to allow more Lyapunov functions than component systems [29], because the same controller using multiple Lyapunov functions can simply be treated as additional controllers. We can add an additional Lyapunov function, $V_{\rm i}' = \alpha V_{\rm i}$, where α is a scalar such that $\alpha V_{\rm i}(\mathbf{e}_{\rm i}(0)) = (1/2)\gamma_{\rm i}^2$. This scaled Lyapunov function will be used only once before the first switch.
- Condition 5 follows from (10).
- Condition 6 follows from the fact that $V_{\rm p}(\mathbf{e}_{\rm p}(t)) = (1/2)\gamma_{\rm p}^2$ for all $t \in \mathcal{T}_{\rm p}$. □

Consider the case that the current state is near the intersection of the boundaries $\gamma_{\rm p}$, and $\gamma_{\rm i}$. While both errors never increase at the same time, the accumulated result of switches can result in a general increase in both errors. In this case the system would head toward the intersection of $\gamma_{\rm i}$ and $\gamma_{\rm p}$. An illustration of such an occurrence, in the space $\mathcal{W}$, is shown in Fig. 2. This does not violate the condition of stability; the system is heading to an accumulation point at the intersection and cannot move past it.

However, the time between switching will become increasingly shorter as the system approaches the intersection. There is no condition on the number of or time between switches, however rapid switching is undesirable. There are several ways to handle this problem. One is to sense when the system is switching too rapidly and enter a "shut down" mode where the robot stops moving. A second method is to impose a minimum time between switches.

A related problem is finite sensor update time. As the time between switches decreases, the system could move from one boundary past the other boundary in less than the sensor update time. Once beyond the switching boundaries, the system has no guarantee of reentering the stable subspace. This problem would likely be exacerbated if a minimum time between switches is imposed.

We address this issue analytically and offer a modification to the system to insure the system slows down near intersections of the switching surfaces and cannot move past the switching surfaces due to a minimum switching time. In order to slow the system near the switching surfaces, we introduce nonlinear, time-varying, scalar gains, K_i and K_p. To simplify the following equations, we define two values $\gamma_{\rm p}' = (1/2)\gamma_{\rm p}^2$ and $\gamma_{\rm i}' = (1/2)\gamma_{\rm i}^2$.

$$K_i = \begin{cases} \frac{\lambda_{\rm i}}{2\|\mathbf{L}_{\rm i}^+\|}\left[\frac{\gamma_{\rm p}' - V_{\rm p}}{\gamma_{\rm p}'} + \frac{\gamma_{\rm i}' - V_{\rm i}}{\gamma_{\rm i}'}\right]; & \|\mathbf{L}_{\rm i}^+\| \geq 1, \\ & V_{\rm i} \leq \gamma_{\rm i}',\ V_{\rm p} \leq \gamma_{\rm p}' \\ \frac{\lambda_{\rm i}}{2}\left[\frac{\gamma_{\rm p}' - V_{\rm p}}{\gamma_{\rm p}'} + \frac{\gamma_{\rm i}' - V_{\rm i}}{\gamma_{\rm i}'}\right]; & \|\mathbf{L}_{\rm i}^+\| < 1, \\ & V_{\rm i} \leq \gamma_{\rm i}',\ V_{\rm p} \leq \gamma_{\rm p}' \\ \lambda_{\rm i}; & \text{else} \end{cases} \quad (21)$$

$$K_p = \begin{cases} \frac{\lambda_\mathrm{p}}{2\|\mathbf{L}_\mathrm{i}\|}\left[\frac{\gamma'_\mathrm{p}-V_\mathrm{p}}{\gamma'_\mathrm{p}}+\frac{\gamma'_\mathrm{i}-V_\mathrm{i}}{\gamma'_\mathrm{i}}\right]; & \|\mathbf{L}_\mathrm{i}\|\geq 1, \\ & V_\mathrm{i}\leq\gamma'_\mathrm{i},\ V_\mathrm{p}\leq\gamma'_\mathrm{p} \\ \frac{\lambda_\mathrm{p}}{2}\left[\frac{\gamma'_\mathrm{p}-V_\mathrm{p}}{\gamma'_\mathrm{p}}+\frac{\gamma'_\mathrm{i}-V_\mathrm{i}}{\gamma'_\mathrm{i}}\right]; & \|\mathbf{L}_\mathrm{i}\|<1, \\ & V_\mathrm{i}\leq\gamma'_\mathrm{i},\ V_\mathrm{p}\leq\gamma'_\mathrm{p} \\ \lambda_\mathrm{p}; & \text{else} \end{cases} \quad (22)$$

where $\|\cdot\|$ for a vector is the standard 2-norm, or Euclidean norm, and for a matrix is the 2-norm and equals the largest singular value of the matrix. Note that K_i and K_p are smooth if $V_\mathrm{i}\leq\gamma'_\mathrm{i}$ and $V_\mathrm{p}\leq\gamma'_\mathrm{p}$. This is true at the initial conditions under the assumptions of the proof, and it remains true for all time at the completion of the proof.

When using IBVS, V_p is a function of $\mathbf{e}_\mathrm{i}$ and $\mathbf{e}_\mathrm{p}$. Using the gain, K_i, defined in (21), along with (6), (9) and (12), and the fact that $\|\mathbf{L}_\mathrm{p}\|=1$ we have

$$\dot{V}_\mathrm{p} = -K_i\mathbf{e}_\mathrm{p}^T\mathbf{L}_\mathrm{p}\mathbf{L}_\mathrm{i}^+\mathbf{e}_\mathrm{i} \quad (23)$$

$$\|\dot{V}_\mathrm{p}\| \leq K_i\left\|\mathbf{L}_\mathrm{i}^+\right\|\|\mathbf{e}\|\|\mathbf{e}_\mathrm{i}\| \quad (24)$$

$$\|\dot{V}_\mathrm{p}\| \leq \lambda_i\frac{\gamma'_\mathrm{p}-V_\mathrm{p}}{\gamma'_\mathrm{p}}\sqrt{V_\mathrm{p}\gamma'_\mathrm{i}}. \quad (25)$$

While IBVS is the active mode, the time-varying gain affects V_i as well. From (21) and (14)

$$\dot{V}_\mathrm{i} = -K_i\mathbf{e}_\mathrm{i}^T\mathbf{L}_\mathrm{i}\mathbf{L}_\mathrm{i}^+\mathbf{e}_\mathrm{i} \quad (26)$$

$$\|\dot{V}_\mathrm{i}\| \leq -K_i\|\mathbf{L}_\mathrm{i}\|\left\|\mathbf{L}_\mathrm{i}^+\right\|\|\mathbf{e}_\mathrm{i}\|^2 \quad (27)$$

$$\|\dot{V}_\mathrm{i}\| \leq -\lambda_i\frac{\gamma'_\mathrm{p}-V_\mathrm{p}}{\|\mathbf{L}_\mathrm{i}^+\|\gamma'_\mathrm{p}}\gamma'_\mathrm{i}, \quad (28)$$

assuming $\|\mathbf{L}_\mathrm{i}^+\|\geq 1$. As expected, while in IBVS mode, $\dot{V}_\mathrm{i}$ remains negative semidefinite, but $\dot{V}_\mathrm{p}$ does not.

It can be shown that $\|\mathbf{L}_\mathrm{i}^+\|$ is bounded from below by some $\beta>0$. However, β will depend on the number of feature points, the relative positions of the feature points, the camera parameters, etc. Due to the uncertainty of the lower bound of $\|\mathbf{L}_\mathrm{i}^+\|$, we bound it at 1 in K_i. It seems this may be unnecessary. Simulation of a sampling of 30,000 error poses about a goal pose gave histograms for values of $\|\mathbf{L}_\mathrm{i}^+\|$ and $\|\mathbf{L}_\mathrm{i}\|$ for 4 points. These are shown in Fig. 3 Both are clearly bounded from below by $\beta>1$.

Assume that at time t_1 the system has just switched to IBVS mode, so $V_\mathrm{i}(t_1)=\gamma'_\mathrm{i}$. Define the minimum update time as t_Δ. We seek to pick a K_i such that

$$V_\mathrm{p}(t_1+t_\Delta)=\dot{V}_\mathrm{p}(t_1)t_\Delta<\gamma'_\mathrm{p}. \quad (29)$$

In the case that the number of feature points is greater than three and $\mathbf{e}_i$ is in the null space of $\mathbf{L}_\mathrm{i}^+$, a subset of three feature points can be temporarily used. It remains to prove that if $\dot{V}_\mathrm{p}$ is positive definite, (29) is satisfied.

$$\dot{V}_\mathrm{p}(t_1)t_\Delta\leq\lambda_i\sqrt{\gamma'_\mathrm{p}\gamma'_\mathrm{i}}\frac{\gamma'_\mathrm{p}-V_\mathrm{p}(t_1)}{\gamma'_\mathrm{p}}t_\Delta\leq\gamma'_\mathrm{p}-V_\mathrm{p}(t_1) \quad (30)$$

$$\lambda_i\sqrt{\frac{\gamma'_\mathrm{i}}{\gamma'_\mathrm{p}}}\left(\gamma'_\mathrm{p}-V_\mathrm{p}(t_1)\right)t_\Delta\leq\gamma'_\mathrm{p}-V_\mathrm{p}(t_1) \quad (31)$$

$$\lambda_i\leq\frac{1}{t_\Delta}\sqrt{\frac{\gamma'_\mathrm{p}}{\gamma'_\mathrm{i}}} \quad (32)$$

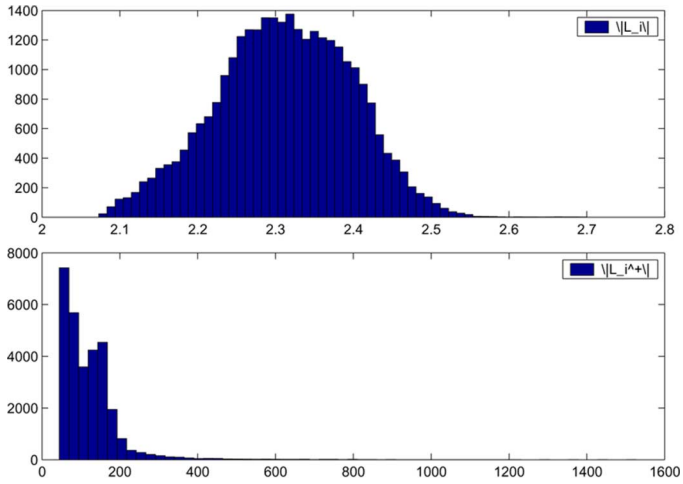

Fig. 3. Histograms of $\|\mathbf{L}_\mathrm{i}^+\|$ and $\|\mathbf{L}_\mathrm{i}\|$ for 4 points.

So the condition in (29) is met if λ_i is sufficiently small. As expected, as the minimum time between switches increases, λ_i decreases to insure a slower velocity.

We have sought a proof of minimum dwell time between switches, but have been unable to prove this. One recurring problem with analysis of visual servoing systems is the inability to find a closed-form solution for the inverse of the image Jacobian, $\mathbf{L}_\mathrm{i}$. This prevents us from saying anything definitive about the effects of IBVS on the pose error, and relegates us to numerical results or imposing bounds on $\mathbf{L}_\mathrm{i}^+$.

Fig. 4 shows a simulation of the trajectory of the errors in $\mathcal{W}$ for a task involving a translation of $[T_x,T_y,T_z]^T=[0.7500,-0.6495,0.3750]^T$ in meters and a rotation of $\theta\mathbf{u}=0.8932[0.1075,-0.4012,-0.9097]^T$ where θ is given in radians. Note that $1/2\|\mathbf{e}_\mathrm{i}(0)\|^2>\gamma_\mathrm{i}$. Fig. 4(a) shows the result for the non-time-varying gain with $\lambda_i=\lambda_p=0.05$ and $\gamma_\mathrm{i}=150$ and $\gamma_\mathrm{p}=0.5$. The system moves far outside the boundaries since the sensor time delay does not detect the boundary until it is past. Fig. 4(b) uses the time-varying gains with $\lambda_i=\lambda_p=0.25$. The system heads to the intersection and becomes stuck there. While this does not alter the stability of the system (the system does not fail due to lost features or task space constraints), failure to converge is not desirable. Fig. 4(c) shows the results for the time-varying gains, but increases γ_p to 0.75. The system now goes to zero error eventually. This suggests that if the state becomes trapped, and the boundaries are known to be conservative, temporarily increasing the boundaries may free it, though careful consideration of the state should be taken first. Further results for the use of the time-varying gains will be given in Section V.

It must be emphasized that this stability proof is a local result, and given the reliance upon the local stability of the IBVS and PBVS controllers, and the existence of a local diffeomorphism between $\mathbf{e}_\mathrm{p}$ and $\mathbf{e}_\mathrm{i}$, the sufficient region of stability may be small. However, this is only a sufficient condition, and in Section V we experimentally demonstrate that the region of stability appears to be quite large. Furthermore, while this proof is only for stability, not asymptotic stability, experiments suggest that the switched system is attractive to the origin over a large region.

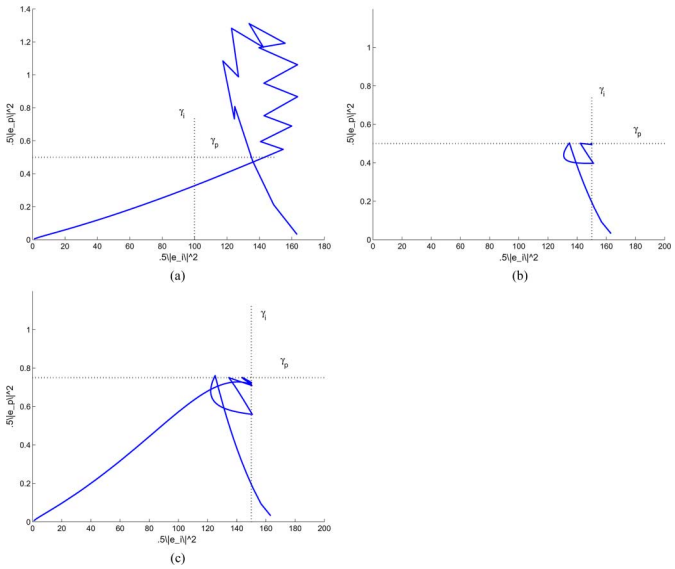

Fig. 4. Simulation of errors in the $\mathcal{W}$ space.

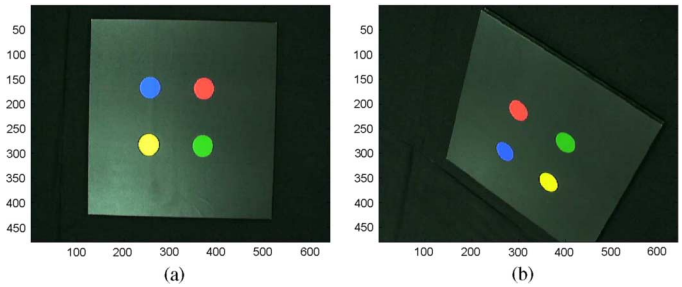

Fig. 5. Initial and goal images.

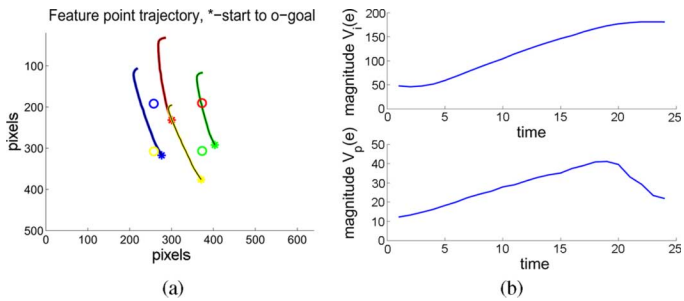

Fig. 6. Experiment of PBVS under large general motion.

One goal of the switching method is to insure that the system never fails due to the robot moving to the end of its reachable space or losing feature points from the image. The choice of γ_{i} and γ_{p} can keep the system from failure, but the best choices may require some knowledge of the goal. The goal image and goal pose must be known for IBVS and PBVS, respectively, so this does not add additional knowledge requirements.

For instance, given n feature points, a conservative γ_{i} is $1/n$ times the least distance from any goal feature point to any edge of the image. While very restrictive, this will guarantee that no feature point can leave the image. If n is large, the feature points are tightly clustered and are roughly centered in the goal image, then γ_{i} can be increased over the conservative estimate. Additionally, knowledge of the goal pose will aid in selecting γ_{p}. If the goal pose is known to be far from the 3D feature points, a large γ_{p} will be necessary.

The switching system can be extended to guard against other common causes of failure as well. Local minima can exist in IBVS, thus if IBVS has zero velocity for a nonzero error, switching to PBVS may free the system from the attraction of the local minimum. Likewise, it is possible to carve out other "forbidden regions" in the image space that correspond to such things as obstacles in the workspace or joint limits in the joint space. If IBVS approaches these regions, the system can switch to PBVS or a joint space control to avoid the region. This topic was explored by Deng, *et al.* [24].

V. Experimental Results

We present experimental results using the state based switching rule. These results support our stability proof and offer insight into the performance characteristics of the system. Calibration of both the camera intrinsic parameters and the extrinsic parameters relating the camera position to the robot end effector are left coarse. This was done intentionally to demonstrate the robustness of the switched-system.

We use IBVS with feature points as described in Section II-C. For PBVS we used epipolar geometry, specifically the homography relating coplanar points in the goal and current camera pose. Planar homography has been used in visual servoing, [10], [12], [37], and specific details can be found in [38].

In our experiment, we used a Puma 560 robot arm and a Sony VW-V500 color camera. The feature targets are the centroids of four colored dots. Depth was estimated using knowledge of the target geometry. Since many of these tasks involve large errors in the image and position, the gains must be kept small or the early motions can be so large as to be potentially damaging for the robot. This also means that when the errors have been mostly reduced the motions are often very small.

We performed many simulations and experiments. For the sake of brevity, we present the results of two difficult tasks. Results for more experiments and simulations are available at [39]. One task involved rotation and translation about all axes. Goal and initial images are shown in Figs. 5(a) and 5(b) respectively.

PBVS results are in Fig. 6. The feature point trajectories, shown in Fig. 6(a), quickly leave the image and the task fails. The values of V_{i} and V_{p} are shown in Fig. 6(b). The effects of coarse calibration are apparent in these graphs as the pose error initially increases under PBVS. Please note the scale of each graph when comparing results.

Results for IBVS are shown in Figs. 7(a) and 7(b). IBVS experiences camera retreat, and in this case fails due to the robot encountering joint limits on its elbow joint. The camera trajectory brings the camera back toward the robot base, and the robot is unable to accommodate this. Coarse calibration affects performance, and image error increases a little. Results for the hybrid system are shown in Figs. 8(a) and 8(b). We set $\gamma_{\mathrm{i}} = 150$ pixels to keep the features in the image surface and set $\gamma_{\mathrm{p}} = 100$ where the translation is measured in mm and rotation in radians. The system switches twice asymptotically, approaching the goal.

As described above, stability is a local property, and the neighborhood proven to ensure stability may be overly con-

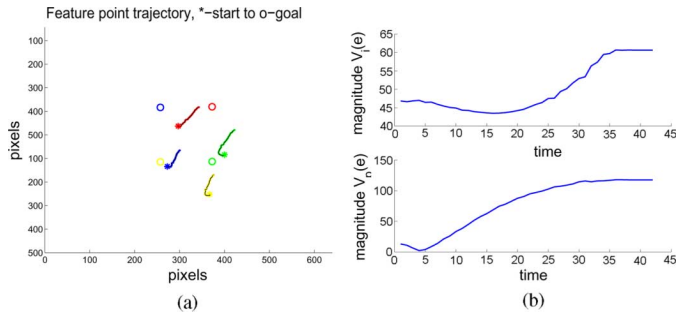

Fig. 7. Experiment of IBVS under large general motion.

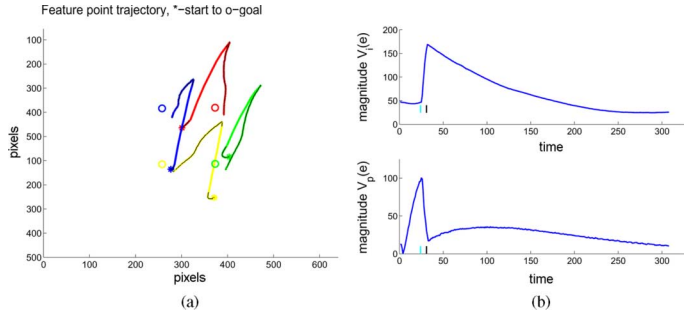

Fig. 8. Experiment of Hybrid VS under large general motion.

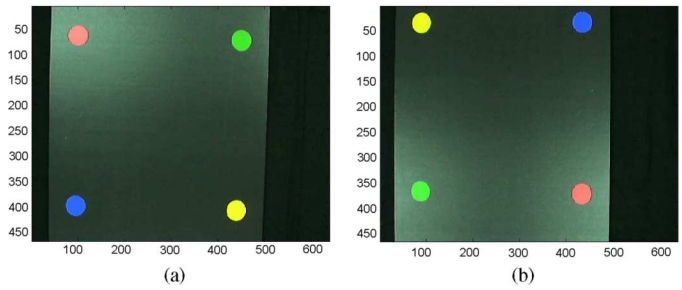

Fig. 9. Initial and goal images.

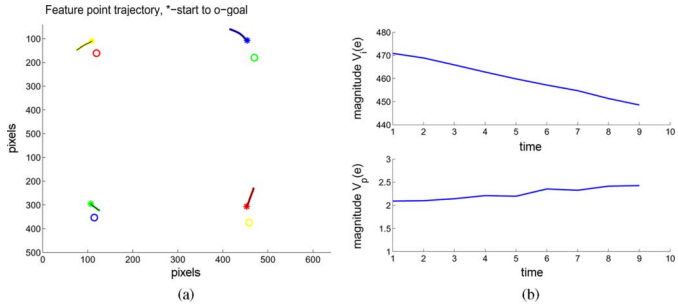

Fig. 10. Experiment of PBVS under large rotation.

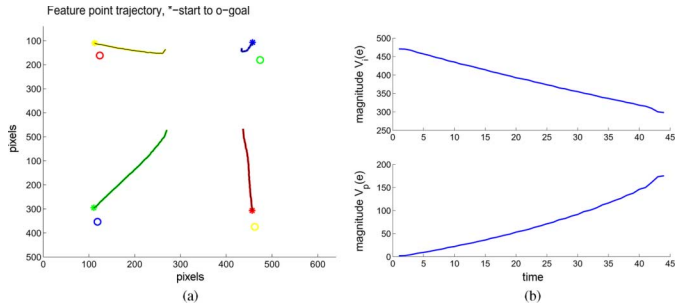

Fig. 11. Experiment of IBVS under large rotation.

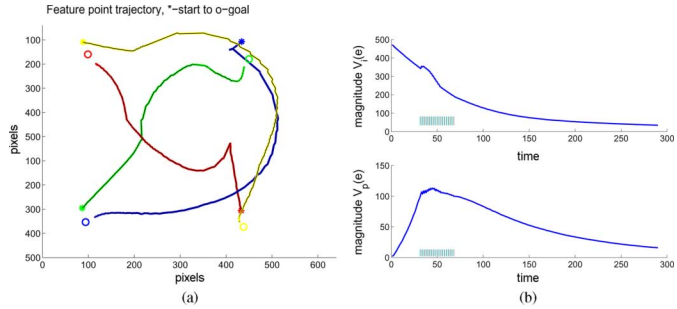

Fig. 12. Experiment of Hybrid VS under large rotation.

servative. We have performed a number of experiments to demonstrate the performance of our system when the initial configuration does not lie in a conservatively defined region of stability. Here, we present the example of a very large rotation about the optical axis, with the feature points close to the edge of the image.

Goal and initial images are shown in Fig. 9. Results of PBVS, IBVS and Hybrid VS are shown in Figs. 10–12. The feature points leave the image under PBVS control. IBVS undergoes severe camera retreat and encounters its joint limits. The Hybrid VS system begins outside the region of stability proven for the switched system in Section IV-B. After undergoing an initial camera retreat, the system encounters $\gamma_{\mathrm{i}} = 100$ and switches to PBVS. PBVS reduces the retreat slightly, but the image error lies outside γ_{p} and the system switches back to IBVS. Rapid switching occurs, during which both the IBVS and PBVS modes reduce the rotation error. Eventually rotation error is reduced to a level that IBVS does not experience camera retreat and the system converges to zero error.

As seen in Fig. 4, it is possible for a system to switch forever and converge to an accumulation point other than the goal. This does not violate the condition of stability, but it is not desirable behavior. Arguably, however, this is preferable to a loss of features or the robot reaching its joint limits.

Empirically, it appears that switching forever, or ending in such an accumulation point happens rarely. We have presented results of that showed attraction to the origin, including when the switched-system visual servoing started outside its proven region of stability. However, this is not conclusive. In an effort to determine how often the system may not reach the goal, we ran Monte Carlo analysis. The results lend strong support to the notion that the system is nearly always attractive to the goal (in our experiments, the system reached the goal 99% of the time using time-varying gains). This analysis also sheds light on the practical performance of the system.

We ran Monte Carlo analysis in simulation for PBVS, IBVS and our switched-system approach using time-varying gains and constant gains. We sampled the six-dimensional configuration space (translation and rotation about three axes), resulting in 30,000 unique initial camera poses with the feature points in front of the camera. Many of these starting poses are outside of the sufficient region of stability of the switched system, in which

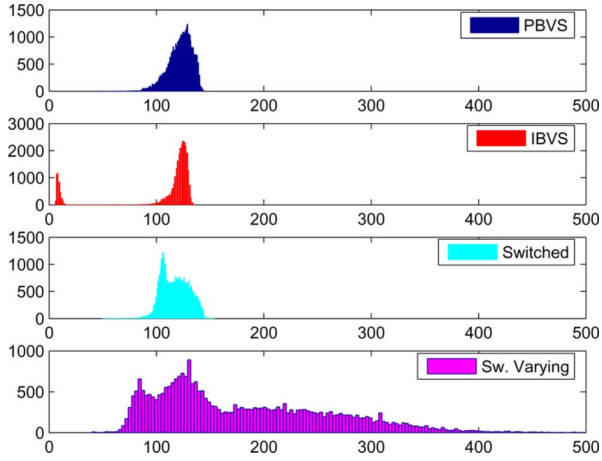

Fig. 13. Histograms of time needed to move to goal pose.

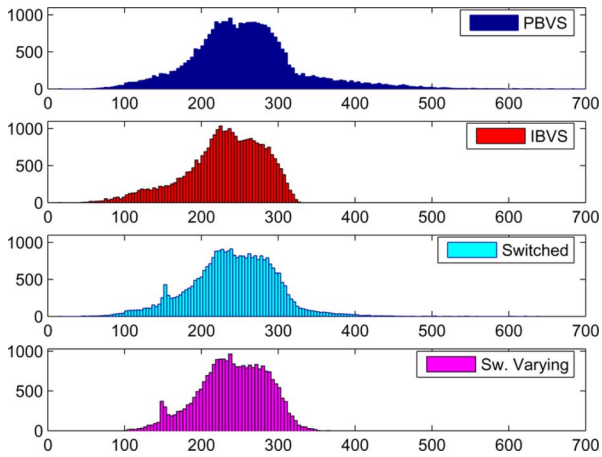

Fig. 14. Histograms for $\|\mathrm{e_i}\|$.

case rapid switching may result. Gains were chosen such that each system completed a series of simple test tasks in about 120 iterations. The thresholds for the switched system (both with and without time-varying gains) are $\gamma_\mathrm{p} = 1000$ and $\gamma_\mathrm{i} = 150$.

For each starting pose, we recorded the time needed for each of these systems to reach the goal pose. Histograms of the time to convergence are seen in Fig. 13. PBVS and the switched system with constant gains have similar distributions. IBVS has several tasks that complete very quickly, but for the majority of tasks it performs similarly to PBVS. The switched system with time-varying gains is notably slower for a number of tasks than the other methods, as the gains will slow it down. Additionally, .97% of the tasks took longer than 5000 iterations to complete. These cases were assumed to be "stuck" at an intersection of the switching surfaces. Such cases were be deemed failures, although the system remains stable.

We also recorded the maximum value of $\|\mathrm{e_p}\|$ and $\|\mathrm{e_i}\|$ encountered during each task. In Figs. 14 and 15 we show histograms of the maximum values encountered. In order to maintain detail, the vertical scales vary between some of the histograms.

For $\|\mathrm{e_i}\|$, PBVS has a maximum $\|\mathrm{e_i}\| > 350$ pixels in many cases. The distribution of the hybrid switched system with constant gains also has a portion of the distribution greater than

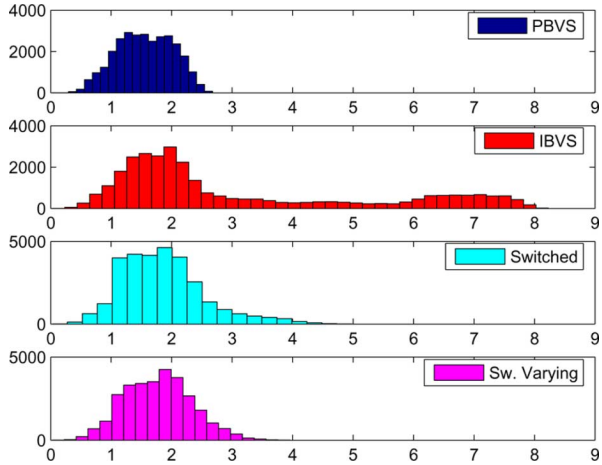

Fig. 15. Histograms for $\|\mathrm{e_p}\|$.

TABLE I
TABLE OF FAILURE RATES

System	Type 1	Type 2	Type 3	Total
PBVS	0%	48.2%	0%	48.2%
IBVS	0%	0%	33.9%	33.9%
Switched	0%	38.8%	11.7%	50.5%
Sw. Varying	0.97%	15.4%	2.5%	18.0%

350 pixels. However, the distribution lies to the left of the distribution for PBVS, indicating an expected lower image error. The distribution of the maximum image error for the switched system with time-varying gains is very close to that of IBVS, indicating few expected failures. If a feature leaves the 512 $\times$ 512 imaging surface, the system was said to fail. Note that the square imaging surface and multiple features means that losing a feature point does not correspond to $\|\mathrm{e_i}\|$ exceeding a specific threshold.

Similarly, for $\|\mathrm{e_p}\|$, IBVS experienced $\|\mathrm{e_p}\|$ greater than three meters for many tasks, while PBVS was never greater than 2.66 meters. For our purposes, $\|\mathrm{e_p}\|$ greater than three meters or less than zero was considered a failure. With constant gains, the switched system experiences several instances where the camera retreat was greater than three meters, though far less than IBVS. The switched system performs much better using the time-varying gains, although some tasks were greater than three meters since many tasks begin outside the sufficient region of stability.

We compile the above info into a set of failure rates. The system was considered to fail in three situations:

1) The system failed to converge within 5000 iterations.
2) A feature point left the image.
3) The system experienced $\|\mathrm{e_p}\| > 3000$, where translation is measured in mm and rotation in radians.

The failure rates are given in Table I. The switched system with time-varying gains outperformed the other systems.

VI. Conclusion

Visual Servoing remains hampered by the fact that no single control method is suitable for all cases. Motivated by this problem, we propose the use of hybrid switched-system control

methods. In this way, a system switches between multiple candidate controllers when it is known that one has an advantage in the current conditions.

We present one such method that incorporates image-based and position-based visual servoing. This is one of the simplest possible switched system visual servo controllers, yet it demonstrates the strength of the idea. We have proven that, within a sufficient neighborhood of the goal, our controller will never fail due to features leaving the image or the camera moving too far from the goal pose. Furthermore, the region of stability is defined by the user, which provides a great deal of control over system performance.

However, this particular system is stable, not asymptotically stable, within part of the region of stability. This introduces the possibility of converging to a point other than the goal, which can be deemed failure. This system also remains susceptible to local minima and singularities in the IBVS control law. Future work will focus on more complicated switched system controllers, possibly integrating controllers besides pure IBVS and PBVS to mitigate these problems.

ACKNOWLEDGMENT

The authors wish to thank the anonymous reviewers for their help in shaping this paper. The authors especially thank the third reviewer for suggestions that resulted in the proof of local asymptotic stability.

REFERENCES

[1] L. E. Weiss, A. C. Sanderson, and C. P. Neuman, "Dynamic sensor-based control of robots with visual feedback," *IEEE Trans. Robot. Automat.*, vol. RA-3, pp. 404–417, Oct. 1987.

[2] J. Feddema and O. Mitchell, "Vision-guided servoing with feature-based trajectory generation," *IEEE Trans. Robot. Automat.*, vol. 5, pp. 691–700, Oct. 1989.

[3] B. Espiau, F. Chaumette, and P. Rives, "A new approach to visual servoing in robotics," *IEEE Trans. Robot. Automat.*, vol. 8, pp. 313–326, Jun. 1992.

[4] K. Hashimoto, Ed., *Visual Control of Robots: High Performance Visual Servoing*. Hong Kong: World Scientific, 1993.

[5] N. P. Papanikolopoulos, P. K. Khosla, and T. Kanade, "Visual tracking of a moving target by a camera mounted on a robot: A combination of vision and control," *IEEE Trans. Robot. Automat.*, vol. 9, no. 1, pp. 14–35, 1993.

[6] P. Martinet, J. Gallice, and D. Khadraoui, "Vision based control law using 3d visual features," in *Proc. WAC 96*, 1996, vol. 3, pp. 497–502.

[7] S. Hutchinson, G. Hager, and P. Corke, "A tutorial on visual servo control," *IEEE Trans. Robot. Automat.*, vol. 12, pp. 651–670, Oct. 1996.

[8] G. S. B. W. J. Wilson and C. C. W. Hulls, "Relative end-effector control using cartesian position based visual servoing," *IEEE Trans. Robot. Automat.*, vol. 12, no. 5, pp. 684–696, 1996.

[9] F. Chaumette, "Potential problems of stability and convergence in image-based and position-based visual servoing," in *The Confluence of Vision and Control*, D. Kriegman, G. Hager, and S. Morse, Eds. : Springer-Verlag, 1998, vol. 237, Lecture Notes in Control and Information Sciences, pp. 66–78.

[10] E. Malis, F. Chaumette, and S. Boudet, "2-1/2d visual servoing," *IEEE Trans. Robot. Automat.*, vol. 15, pp. 238–250, Apr. 1999.

[11] G. Morel, T. Liebezeit, J. Szewczyk, S. Boudet, and J. Pot, "Explicit incorporation of 2d constraints in vision based control of robot manipulators," in *Experimental Robotics VI*, P. Corke and J. Trevelyan, Eds. : Springer-Verlag, 2000, vol. 250, Lecture Notes in Control and Information Sciences, pp. 99–108, 1 85233 210 7.

[12] K. Deguchi, "Optimal motion control for image-based visual servoing by decoupling translation and rotation," in *Proc. Int. Conf. Intelligent Robots and Systems*, Oct. 1998, pp. 705–711.

[13] P. Corke and S. Hutchinson, "A new partitioned approach to image-based visual servo control," *IEEE Trans. Robot. Automat.*, vol. 17, no. 4, pp. 507–515, 2001.

[14] C. Taylor and J. Ostrowski, "Robust vision-based pose control," in *Proc. Int. Conf. Robot. Automat.*, 2000, pp. 2734–2740.

[15] N. Cowan, J. Weingarten, and D. Koditschek, "Visual servoing via navigation functions," *IEEE Trans. Robot. Automat.*, vol. 18, no. 4, pp. 521–533, 2002.

[16] Y. Mezouar and F. Chaumette, "Path planning in image space for robust visual servoing," in *Proc. Int. Conf. Robot. Automat.*, 2000, pp. 2759–2764.

[17] V. Kyrki, D. Kragic, and H. Christensen, "Path planning in image space for robust visual servoing," in *Proc. Int. Conf. Intelligent Robots and Systems*, 2004, pp. 349–354.

[18] N. Garcia-Aracil, E. Malis, R. Aracil-Santonja, and C. Perez-Vidal, "Continuous visual servoing despite the changes of visibility in image features," *IEEE Trans. Robotics*, vol. 21, no. 6, pp. 1214–1220, 2005.

[19] N. R. Gans and S. A. Hutchinson, "A switching approach to visual servo control," in *Proc. IEEE Int. Symp. Intell. Control*, 2002.

[20] N. Gans and S. Huthcinson, "An experimental study of hybrid switched system approaches to visual servoing," in *Proc. Int. Conf. Robot. Automat.*, May 2003.

[21] M. Branicky, V. Borkar, and S. Mitter, "A unified framework for hybrid control," in *Proc. 33rd IEEE Conf. Decision and Control*, 1994.

[22] R. W. Brockett, *Hybrid Models for Motion Control Systems*, H. L. Trentelman and J. C. Willems, Eds. : Birkhauser, 1993.

[23] G. Chesi and A. Vicino, "Visual servoing for large camera displacements," *IEEE Trans. Robot. Automat.*, vol. 20, no. 4, pp. 724–735, 2004.

[24] L. Deng, F. Janabi-Sharifi, and W. Wilson, "Hybrid motion control and planning strategies for visual servoing," *IEEE Trans. Ind. Electron.*, vol. 52, no. 4, pp. 1024–1040, 2005.

[25] B. Nelson and P. Khosla, "Strategies for increasing the tracking region of an eye-in-hand system by singularity and joint limit avoidance," *Int. J. Robot. Res.* vol. 14, Jun. 1995 [Online]. Available: /afs/cs/user/bnelson/ftp/ijrr.sjl.ps.Z

[26] F. Chaumette and T. Marchand, "A redundancy-based iterative approach for avoiding joint limits: Application to visual servoing," *IEEE Trans. Robot. Automat.*, vol. 17, no. 5, pp. 719–730, 2001.

[27] D. Liberzon and A. Morse, "Basic problems in stability and design of switched systems," *IEEE Control Syst. Mag.*, vol. 19, no. 5, pp. 59–70, Oct. 1999.

[28] D. Liberzon, *Switching in Systems and Control*. New York: Birkhauser, 2003.

[29] M. Branicky, "Stability of hybrid systems: State of the art," in *Proc. IEEE Conf. Decision and Control*, 1997, pp. 120–125.

[30] M. Wicks, P. Peleties, and R. DeCarlo, "Construction of piecewise lyapunov functions for stabilizing switched systems," in *Proc. Conf. Decision and Control*, 1994, pp. 3492–3497.

[31] M. Branicky, "Multiple Lyapunov functions and other analysis tools for switched and hybrid systems," *IEEE Trans. Automat. Contr.*, vol. 43, pp. 475–482, 1998.

[32] O. Faugeras and F. Lustman, "Motion and structure from motion in a piecewise planar environment," *Int. J. Pattern Recognit. Artificial Intell.*, vol. 2, no. 3, pp. 485–508, 1988.

[33] Z. Zhang and A. R. Hanson, "3d reconstruction based on homography mapping," in *ARPA Image Understanding Workshop*, Palm Springs, CA, 1996.

[34] D. DeMenthon and L. S. Davis, "Model-based object pose in 25 lines of code," in *Proc. Eur. Conf. Computer Vision*, 1992, pp. 335–343.

[35] L. Deng, F. Janabi-Sharifi, and W. Wilson, "Stability and robustness of visual servoing methods," in *Proc. IEEE Conf. Robot. Automat.*, 2002.

[36] R. Kelly, R. Carelli, O. Nasisi, B. Kuchen, and F. Reyes, "Stable visual servoing of camera-in-hand robotic systems," *IEEE/ASME Trans. Mechatronics*, vol. 5, no. 1, pp. 39–48, Mar. 2000.

[37] Y. Fang, W. Dixon, D. Dawson, and P. Chawda, "Homography-based visual servo regulation of mobile robots," *IEEE Trans. Syst., Man Cybern.*, vol. 35, no. 5, pp. 1041–1050, 2005.

[38] O. Faugeras and F. Lustman, "Motion and structure from motion in a piecewise planar environment," *Int. J. Pattern Recognit. Artificial Intell.*, vol. 2, no. 3, pp. 485–508, 1988.

[39] F. Chaumette, "Switched system visual servo control," Ph.D. dissertation, Univ. Illinois, Urbana-Champaign, 2005.

Nicholas R. Gans (M'02) received the B.S. degree from Case Western Reserve University, Cleveland, OH, in 1999, and the M.S. and Ph.D. degrees from the University of Illinois Urbana-Champaign, Urbana, IL, in 2002 and 2005, respectively.

He is currently a Postdoctoral Researcher at the University of Florida, working with both the Nonlinear Control and Robotics Laboratory in Gainesville, FL, and the Research and Engineering Education Facility in Shalimar, FL. His research interests include visual servoing, vision-based control, and nonlinear control of robot systems.

Seth A. Hutchinson (F'06) received the Ph.D. from Purdue University, West Lafayette, IN, in 1988.

In 1990 he joined the faculty at the University of Illinois in Urbana-Champaign, where he is currently a Professor in the Department of Electrical and Computer Engineering, the Coordinated Science Laboratory, and the Beckman Institute for Advanced Science and Technology. He has published more than 100 papers on the topics of robotics and computer vision, and is coauthor of the books *Principles of Robot Motion: Theory, Algorithms, and Implementations* (MIT Press, 2005), and *Robot Modeling and Control* (Wiley, 2006).

Dr. Hutchinson serves as the Editor-in-Chief for the RAS Conference Editorial Board, and on the editorial boards of the *International Journal of Robotics Research* and the *Journal of Intelligent Service Robotics*. He served as Associate and then Senior Editor for the IEEE TRANSACTIONS ON ROBOTICS AND AUTOMATION, now the IEEE TRANSACTIONS ON ROBOTICS, from 1997 to 2005. In 1996 he was a guest editor for a special section of the Transactions devoted to the topic of visual servo control, and in 1994 he was co-chair of an IEEE Workshop on Visual Servoing. In 1996 and 1998 he co-authored papers that were finalists for the King-Sun Fu Memorial Best Transactions Paper Award. He was co-chair of IEEE Robotics and Automation Society Technical Committee on Computer and Robot Vision from 1992 to 1996, and has served on the program committees for more than 50 conferences related to robotics and computer vision.